AGU PUBLICATIONS

Geophysical Research Letters

RESEARCH LETTER
10.1002/2015GL064707

Key Points:
- We find the best specification for ULF wave radial diffusion in Van Allen Belts
- Storm-time ULF waves have a stronger Kp dependence than solar cycle average
- Proposed new two parameter Kp-Dst wave specification has huge modeling impacts

Correspondence to:
S. Dimitrakoudis,
sdimis@noa.gr

Citation:
Dimitrakoudis, S., I. R. Mann, G. Balasis, C. Papadimitriou, A. Anastasiadis, and I. A. Daglis (2015), Accurately specifying storm-time ULF wave radial diffusion in the radiation belts, *Geophys. Res. Lett.*, *42*, 5711–5718, doi:10.1002/2015GL064707.

Received 26 MAY 2015
Accepted 27 JUN 2015
Accepted article online 1 JUL 2015
Published online 23 JUL 2015

Accurately specifying storm-time ULF wave radial diffusion in the radiation belts

Stavros Dimitrakoudis[1], Ian R. Mann[2], Georgios Balasis[1], Constantinos Papadimitriou[1,3], Anastasios Anastasiadis[1], and Ioannis A. Daglis[1,3]

[1]National Observatory of Athens, Institute for Astronomy, Astrophysics, Space Applications and Remote Sensing, Penteli, Greece, [2]Department of Physics, University of Alberta, Edmonton, Alberta, Canada, [3]Section of Astrophysics, Astronomy and Mechanics, Department of Physics, University of Athens, Athens, Greece

Abstract Ultralow frequency (ULF) waves can contribute to the transport, acceleration, and loss of electrons in the radiation belts through inward and outward diffusion. However, the most appropriate parameters to use to specify the ULF wave diffusion rates are unknown. Empirical representations of diffusion coefficients often use *Kp*; however, specifications using ULF wave power offer an improved physics-based approach. We use 11 years of ground-based magnetometer array measurements to statistically parameterize the ULF wave power with *Kp*, solar wind speed, solar wind dynamic pressure, and *Dst*. We find that *Kp* is the best single parameter to specify the statistical ULF wave power driving radial diffusion. Significantly, remarkable high energy tails exist in the ULF wave power distributions when expressed as a function of *Dst*. Two-parameter ULF wave power specifications using *Dst* as well as *Kp* provide a better statistical representation of storm-time radial diffusion than any single variable alone.

1. Introduction

Ultralow frequency (ULF) waves in the magnetosphere have long been suggested as a likely factor affecting the acceleration and diffusion of electrons in the outer radiation belt [e.g., *Fälthammar*, 1965; *Schulz and Lanzerotti*, 1974; *Fei et al.*, 2006]. ULF wave power measurements on the ground or in situ have led to various attempts to derive an analytic expression for their effect on the diffusion coefficient of particles, as a function of some geophysical index or solar wind parameter [e.g., *Brautigam and Albert*, 2000; *Brautigam et al.*, 2005; *Ozeke et al.*, 2012, 2014].

The choice of which solar wind or geophysical parameter or parameters should be used to most accurately specify the ULF wave power, and thereby, the radial diffusion coefficients is important but not yet well understood. For example, the often used radial diffusion coefficient specification presented by *Brautigam and Albert* [2000] parameterizes the diffusion by *Kp*. Similarly, according to the approach of *Brizard and Chan* [2001], the radial diffusion coefficients are proportional to the power spectral density of ULF waves (see also *Fei et al.* [2006]) such that parameterizations of ULF wave power can be used to specify the radial diffusion coefficients.

In this regard, it has been shown for example that solar wind speed (V_{sw}) correlates with ULF power in the Pc3 to Pc5 frequency range (1.7 to 100 mHz) [e.g., *Greenstadt et al.*, 1979; *Mathie and Mann*, 2000; *Pahud et al.*, 2009; *Simms et al.*, 2010; *Rae et al.*, 2012], with a likely physical mechanism being the generation of shear flow instabilities along the magnetopause [*Cahill and Winckler*, 1992; *Mann et al.*, 1999; *Mathie and Mann*, 2000]. Solar wind dynamic pressure changes (P_{dyn}) have also been found to be correlated with ULF wave excitation [e.g., *Kepko et al.*, 2002; *Takahashi and Ukhorskiy*, 2007; *Kessel*, 2008], possibly due to the generation of compressional waves that transmit their energy to field line resonances in the inner magnetosphere [*Kivelson and Southwood*, 1988; *Lysak and Lee*, 1992; *Mann et al.*, 1995; *Hartinger et al.*, 2011]. However, the nature of ULF wave excitation during magnetic storms is not fully understood. For example, the morphology of the storm-time magnetosphere, as well as the solar wind structures which drive storm-time ULF waves such as interplanetary coronal mass ejections or fast solar wind streams/corotating interaction regions, may be different from the conditions that prevail during nominal conditions. Consequently, the ULF wave response of the system may be different during storm and nonstorm times.

In this letter we present a study of 11 years of ground-based magnetometer observations of ULF waves by the International Monitor for Auroral Geomagnetic Effects (IMAGE) array, binned by four parameters: *Kp*, *Dst*, solar

wind dynamic pressure, P_{dyn}, and solar wind speed, V_{sw}. We first examine the distribution of the ULF wave power as a function of these parameters alone, to analyze which parameter might be most appropriate for the statistical representation of ULF wave power. The distributions of ULF wave power reveal that they have a very strong high energy tail. We hence further analyse the ULF wave power distribution as a function of multiple parameters, in particular to examine whether the storm-time disturbance index, *Dst*, should be used in addition to other parameters, such as *Kp* or V_{sw} which have more traditionally been used to parameterize ULF wave power and hence radial diffusion in the outer radiation belt.

In section 2 we describe our data set and processing method; in section 3 we present our results, and we conclude in section 4 with a summary and a short discussion.

2. Data Processing

The power spectra used in this study are derived from 11 years of magnetic field measurements from nine stations in the IMAGE (International Monitor for Auroral Geomagnetic Effects) magnetometer array [*Tanskanen*, 2009] (1 January 2000 to 31 December 2010): Uppsala, Nurmijärvi, Dombås, Oulujärvi, Rørvik, Sodankylä, Kiruna, Kevo, and Tromsø. The particular stations analyzed were chosen on the basis of three conditions: (a) spanning a large range of geomagnetic latitude, (b) spanning a small range of geomagnetic longitude, and (c) > 95% data coverage within our selected time period. We analyzed measurements of the *D* (east) component of the magnetic field, sampled at 10 s cadence, and performed the continuous wavelet transform with a Morlet mother function to derive hourly power spectra [*Balasis et al.*, 2012, 2013]. The frequencies used were selected in the range from 0.6 to 19.85 mHz, spaced with a uniform linear step of 0.25 mHz (chosen for easy comparison with [*Ozeke et al.*, 2012], which used fast Fourier Transform with a similar frequency step). These cover the Pc5 (up to 7 mHz) and Pc4 (7 to 20 mHz) frequency ranges. To remove most impacts from spectral features in the Pc4 and Pc5 ULF band which do not correspond to waves in the equatorial plane, such as nightside substorm bays, we only analyzed data from daytime hours from 0600 to 1800 MLT. We made use of the *D* component of the ground magnetic field measurements because it can be mapped to the azimuthal electric field in space assuming an Alfvénic mode and a 90° rotation through the ionosphere, which is then used to calculate the electric term of the radial diffusion coefficient [*Ozeke et al.*, 2012]. The mapping procedure we used [*Ozeke et al.*, 2009] assumes a dipole geometry for the magnetic field, which is problematic as an approximation for the nightside of the magnetosphere; but this is somewhat mitigated by our exclusive use of daytime measurements.

The ULF wave power measurements were then binned with *Kp*, V_{sw}, P_{dyn}, and *Dst* using data from the OMNI database [*King and Papitashvili*, 2005] at hourly resolution. In order to robustly compare the relative efficacy of each binning parameter, we divided the data set into 10 equal deciles, ensuring that each bin for each different driving parameter has the same number of data points. Table 1 shows the lowest and highest values of the parameters during the period of observation, as well as the values that denote the borders of their respective deciles. The total number of days is 4013, since there is a 5 day gap in ULF measurement data from early 2000, which means we have 48,216 daylight hours of data in total, and up to 4816 hourly spectra in each decile.

Since the OMNI solar wind database is not complete for this interval, each V_{sw} decile has only 4809 data points, while each P_{dyn} decile has 4768 data points. The difference in bin sizes, with the ones for V_{sw} being 0.14% smaller and the ones for P_{dyn} being 1% smaller than the ones for *Kp* and *Dst* can be considered to be statistically negligible. The total number of daylight hours for each station is further affected by small data gaps interspersed throughout the 11 years, with up to 5% fewer hours in the case of Rørvik station. Such gaps have no effect on the relative size of the decile bins for each station, and assuming the data gaps are randomly distributed, they will only have a very small effect on the statistical comparisons from station to station.

As shown below, the data demonstrate that the ULF wave power distributions have long high power tails, including for *Dst*. In the case of *Dst* we further calculate the highest ten percentiles, splitting the highest *Dst* decile further into 10 percentile bins in order to examine the storm-time variations of ULF wave power. Finally, we also derive two-dimensional probability distributions, to both examine the utility of using two parameter ULF wave specifications and to look for differences between ULF wave power during storm and storm times.

Table 1. Decile Borders for Each Binning Parameter: *Kp*, Solar Wind Speed (V_{sw}), Solar Wind Dynamic Pressure (P_{dyn}), and *Dst*

Decile border	*Kp*	V_{sw} (km/s)	P_{dyn} (nPa)	*Dst* (nT)
0	0	233	0.03	67
1	0.3	320	0.81	6
2	0.7	346	1.01	1
3	1	369	1.19	−2
4	1.3	393	1.36	−6
5	1.7	418	1.57	−9
6	2	448	1.81	−13
7	2.7	485	2.14	−18
8	3	537	2.61	−25
9	3.7	607	3.54	−35
10	9	1189	79.05	−422

3. Dependence of ULF Wave Power on the Selected Parameters

Figure 1 shows the mean power spectral densities (PSDs) and their standard errors in each decile for Nurmijärvi (NUR) station at $L = 3.4$ (geomagnetic longitude 102.18°), for all four parameters used in this study, while Figure 2 shows the same parameters for the Tromsø (TRO) station at $L = 6.46$ (geomagnetic longitude 102.9°). These stations span from midlatitude to close to geosynchronous orbit, with L values which span the outer radiation belt. The following traits stand out (which also apply to the observations from the intermediate latitude stations and which are not shown):

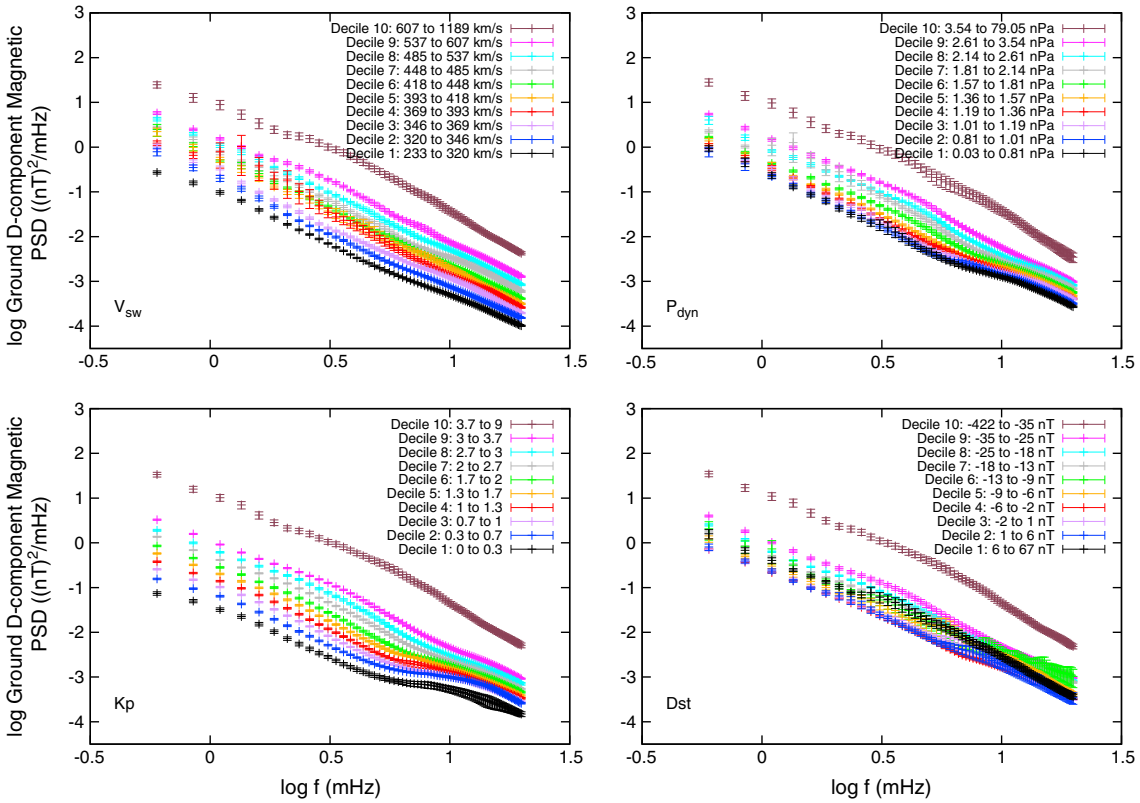

Figure 1. A comparison of mean magnetic field *D* component power spectral densities as measured at Nurmijärvi station ($L = 3.4$), when binned by deciles, with *Kp*, solar wind speed, solar wind pressure, and *Dst*. The error bars show the standard error.

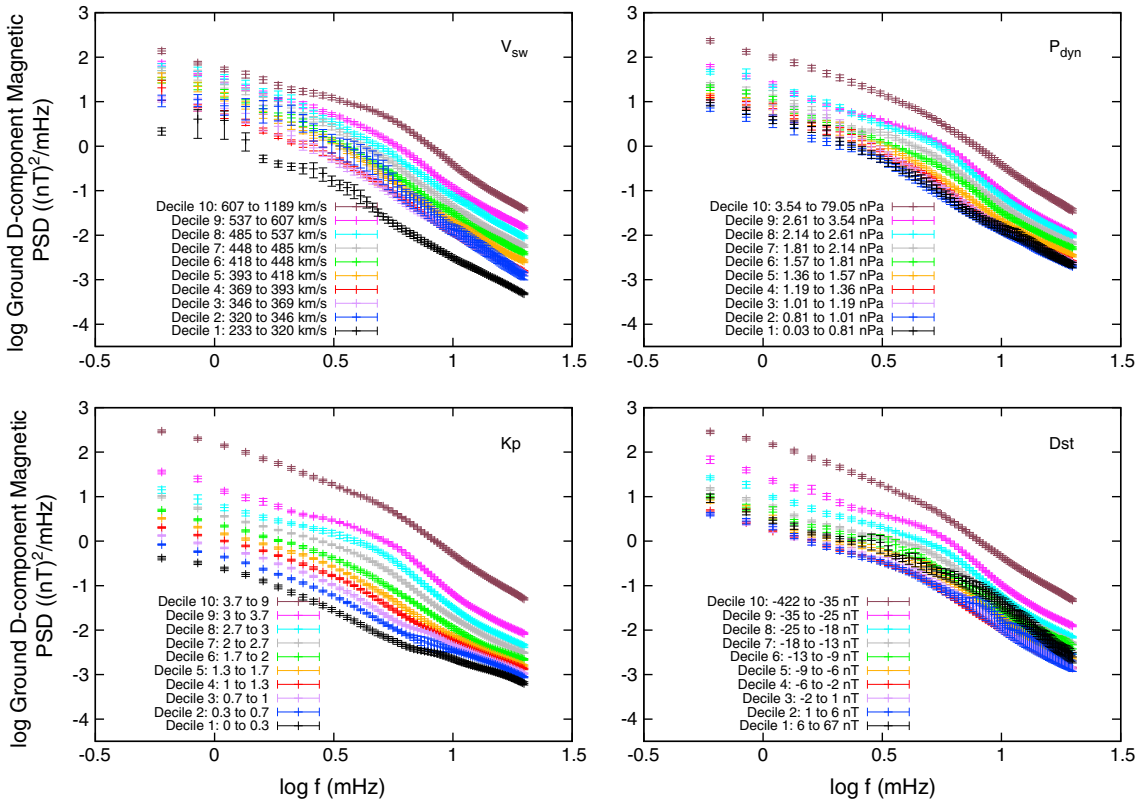

Figure 2. As in Figure 1 but for Tromsø station ($L = 6.46$).

1. Binning by *Kp* provides the largest span in mean power, with smallest standard error in each decile, particularly in the Pc5 frequency range and hence represents the best single parameter with which to specify radial diffusion. Binning by V_{sw} maintains a good span and has utility for radial diffusion simulations as well; the deciles of P_{dyn} and *Dst* do not provide good discriminators of ULF wave power; however, the ULF power in the tenth *Dst* decile is examined further below.
2. The tenth decile of the *Dst* distributions is clearly separated from the others, such that the mean of the 1–9 deciles are very similar, but ULF wave power increases significantly once $Dst < -35$ nT. P_{dyn} shows similar behavior; indeed, the high energy tail of the ULF wave power distribution can also be seen in the *Kp* and the V_{sw} distributions as well. Perhaps more significantly, the separation of the tenth *Dst* decile from the remainder of the distribution is more pronounced at the lower *L* station suggesting the impact of the storm-time dependence of ULF wave power might be relatively larger toward the inner edge of the outer belt.
3. There is also evidence, especially at the high *L* station, for a local enhancement in the frequency spectrum of the ULF wave power above a simple power law, which most likely indicates the impact of ULF wave power accumulation at the local field line resonance [cf. *Rae et al.*, 2012].

This *L* dependence of the ULF power is explored in more detail in Figure 3a, where we have integrated the power spectral density profile for each decile across the Pc5 frequency range and derived the ratio Y_i of the power carried by the upper decile to the total power, where *i* refers to the binning parameter. In the Pc5 frequency range, for *Kp* and *Dst* we see a change in Y_i at around $L = 4.7$ and for P_{dyn} and V_{sw} at around $L = 4.3$, which nevertheless have the same effect: a decrease of Y_i with *L* in the outer magnetosphere. This emphasizes the strength of the high power tail, especially at low *L*. This behavior likely reflects on the physical mechanisms behind the generation of the Pc4 and Pc5 ULF wave; however, a detailed discussion of this is beyond the scope of the current study. Nonetheless, it shows that the ULF wave power distributions are dominated by a high power tail. Figure 3b examines the nature of the high ULF wave power tail by further splitting the top decile into 10 percentiles. What is incredibly clear is that not only are magnetic storms with large *Dst* magnitude associated with very large ULF wave power but also the ULF wave power defined on the basis of an 11 year

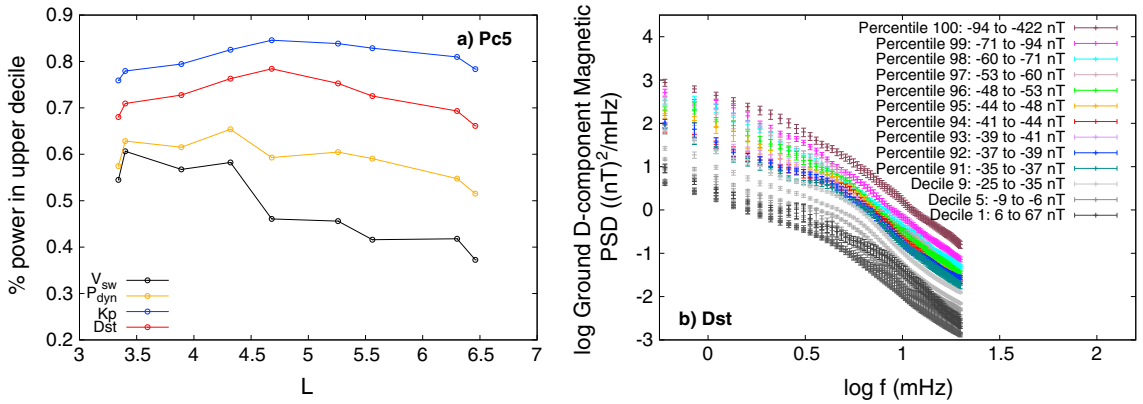

Figure 3. (a) Percentage of total power in the upper decile, for the Pc5 frequency range, for all four binning parameters and for all stations. (b) Mean magnetic field *D* component power spectral densities as measured at Tromsø station ($L = 6.46$), binned by *Dst* as in Figure 2, except that the top decile is further split into percentiles (denoted by 91–100). The lower nine deciles are plotted in grayscale (only three of them, deciles 1, 5, and 9, appear in the legend, as indicative of the color progression).

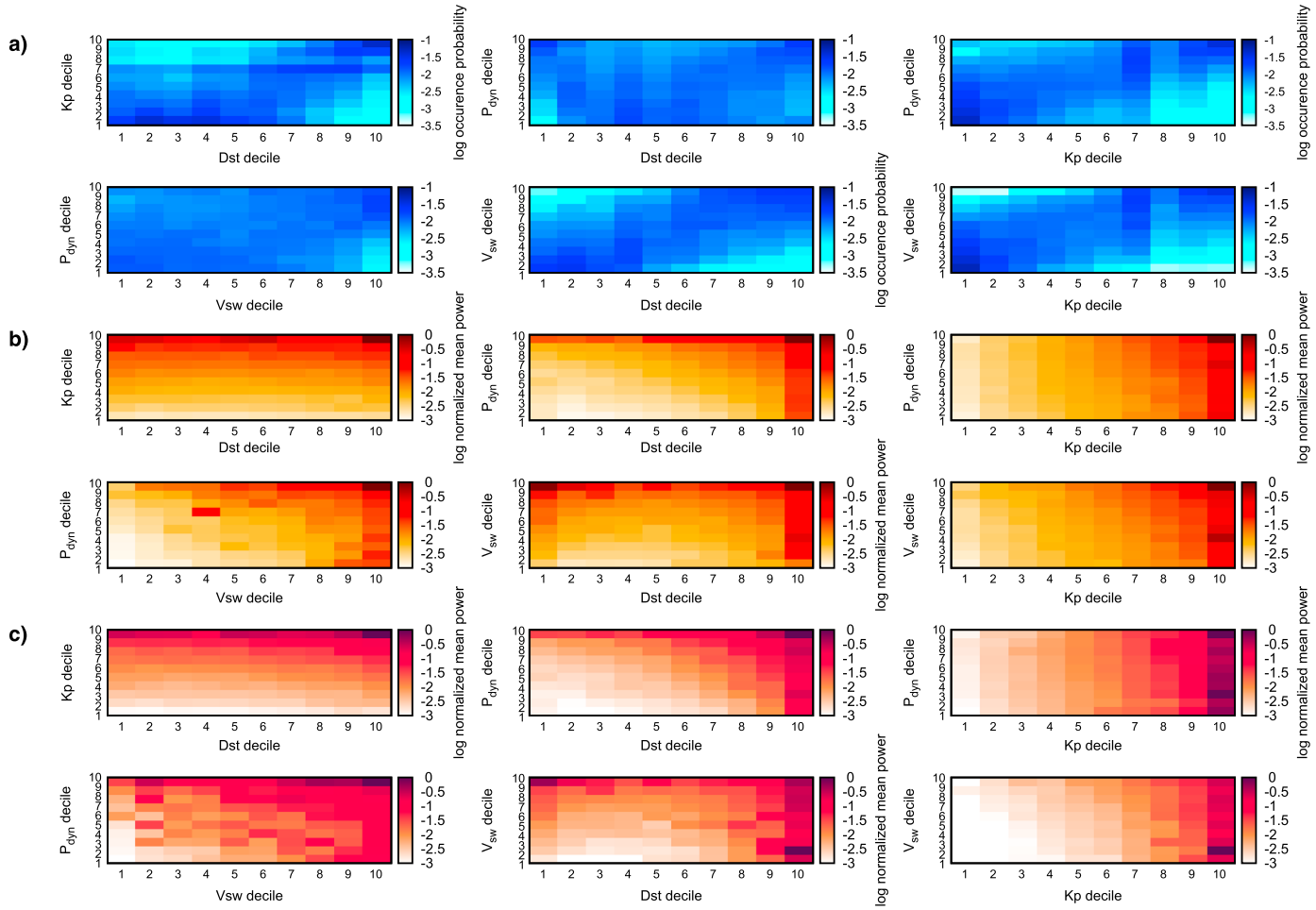

Figure 4. (a) Occurrence probability distributions for pairs of deciles of combinations of the parameters *Kp*, V_{sw}, P_{dyn}, and *Dst*. (b) Mean ULF wave power for each pair of deciles, as in Figure 4a, for Nurmijärvi (NUR) station. (c) Same as Figure 4b but for Tromsø (TRO) station.

database remains well ordered by the *Dst* parameter even at the percent level in this high power tail. Overall, this suggests that studies of the impacts of ULF waves in the radiation belts during magnetic storms should additionally include the *Dst* index together with another parameter, such as *Kp*, when specifying the ULF wave diffusion rates. Such an approach may provide an improved ULF wave power specification for the purposes of modeling radial diffusion.

Figure 4 shows occurrence probability distribution (Figure 4a) as well as the mean ULF wave power in each bin as a function of pairs of deciles of two of the parameters *Kp*, V_{sw}, P_{dyn}, and *Dst* for the NUR (Figure 4b) and TRO (Figure 4c) stations. Figure 4a provides an indication of the parts of the distribution with reliable statistics, and in Figures 4b and 4c the mean power is normalized to the bin with maximum mean power. Figures 4b and 4c show that the range of mean ULF wave power is very large, spanning 3 orders of magnitude. As can be clearly seen in this figure, *Kp* is an excellent discriminator of ULF wave power, with some evidence that conditions of higher V_{sw} and P_{dyn} also contribute additionally to higher ULF wave power for given *Kp*. It is also very clear that more negative *Dst* also contributes to higher ULF power, especially at the lower *L* station. Recall that the highest value of *Dst* in the tenth *Dst* decile has the value of −35 nT (cf. Table 1) such that effectively, all storm times are captured in this decile (cf. also the percent level discrimination of the ULF wave power as a function of *Dst* shown in Figure 3b). Significantly, this indicates that the storm time magnetosphere on average has significantly elevated ULF wave power for the same activity index, e.g., *Kp*, as compared to nonstorm times.

We have also verified that the data analysis presented here using data from the IMAGE magnetometer array and the Morlet wavelet to characterize the ULF wave power reproduces the electric field diffusion coefficients reported in *Ozeke et al.* [2012] and which were derived using data largely from the Canadian Array for Realtime InvestigationS of Magnetic Activity [*Mann et al.*, 2008] and a fast Fourier transform approach. The details will be reported in a more extensive publication elsewhere.

4. Summary and Discussion

We have presented a new statistical analysis of the connection between ULF wave activity in the magnetosphere and four solar wind and geomagnetic index driving parameters (*Kp*, solar wind speed, solar wind dynamic pressure, and *Dst*) using ground-based magnetometer observations of ULF wave power spanning one solar cycle. Unlike a similar study undertaken by *Huang et al.* [2010], which evaluated the effect of various parameters on ULF waves in geostationary orbit, our focus on the D component of multiple ground magnetometer measurements allowed us to probe the power going into the electric term of radial diffusion, at *L* shells covering the full width of the outer radiation belt. Although *Huang et al.* [2010] focused on magnetic field measurements with a linear binning method, which does not allow for casual comparisons with our results even when those are for an *L* shell corresponding to geosynchronous orbit, it is worth noting that they also observed a correlation of the increase of ULF power with increases of *Kp*, *Dst*, and V_{sw}. Since the ULF wave electric field diffusion usually dominates over the magnetic field diffusion [e.g., *Ozeke et al.*, 2012; *Tu et al.*, 2012], then our results have significant implications for the most appropriate specification of the ULF wave power, and hence, the radial diffusion rates in the outer electron radiation belt. We conclude that of these single parameters *Kp* provides the best capability to represent the dynamic range of ULF wave power, which is driven in the magnetosphere. Furthermore, it becomes apparent that the ULF wave power present during magnetic storms (as characterized by *Dst*, which measures the average magnetic depression near the equator as a result of the ring current formed by such storms) is not the same as that averaged over the entire solar cycle. We show conclusively that the level of ULF wave power present in the magnetosphere is larger at storm times than at nonstorm times for the same level of driving conditions, at least as specified by *Kp* (which measures the average global field disturbances), solar wind speed, and solar wind dynamic pressure drivers. As a result, we conclude that including *Dst* as an additional parameter provides an improved method for specifying the ULF wave power and hence the rate of ULF-wave radial diffusion in the radiation belts. We suggest that future studies should examine ULF wave power characterizations which use both *Kp* and *Dst* to specify the power and, as such, could be compared to studies which use the observed ULF wave power in individual storms to drive diffusion. Future studies could additionally examine the ULF wave power relationship to whether the magnitude of *Dst* is increasing or decreasing—thereby examining the statistical differences between ULF wave excitation in the main and recovery phases of magnetic storms.

It has been shown in the past [e.g., *Loto'Aniu et al.*, 2006; *Mann et al.*, 2012] that ULF wave power penetration to low *L* is connected with decreases in *Dst*. Here that is seen with greater clarity, since at low *L* the ULF wave

power comes predominantly from the upper decile of *Dst* measurements, which corresponds to $Dst < -35$ nT, while at high *L* the rest of the deciles have a larger contribution to the overall dynamic range of ULF wave power. Significantly, since ground PSD measurements of ULF waves can be directly translated to the electric term of the radial diffusion coefficient on the equatorial plane in space [e.g., *Ozeke et al.*, 2012], our results have implications for the most appropriate parameters to use for characterizing ULF wave driven radial diffusion. Accurate specification of such diffusive transport rates, especially at the inner edge of the outer radiation belts, will likely be crucial for developing a physical understanding of the nature of the penetration of ULF wave power to low *L* [cf. *Loto'Aniu et al.*, 2006]. Such analyses may also shed light on the physical processes responsible for the reported correlations between the location of this inner boundary and the plasmapause [e.g., *Li et al.*, 2006] (itself correlated with *Dst* see, e.g., *O'Brien and Moldwin* [2003]), as well as the recent reports of the apparently largely impenetrable nature of the inner edge of the outer belt *Baker et al.* [2014].

Acknowledgments

This work has received funding from the European Union's Seventh Framework Programme (FP7-SPACE-2011-1) under grant agreement n. 284520 for the MAARBLE (Monitoring, Analyzing and Assessing Radiation Belt Loss and Energization) collaborative research project. We acknowledge support from the "Hellenic National Space Weather Research Network" cofinanced by the European Union (European Social Fund ESF) and Greek national funds through the Operational Program "Education and Lifelong Learning" of the National Strategic Reference Framework (NSRF) Research Funding Program "Thales. Investing in knowledge society through the European Social Fund". We also acknowledge the use of NASA/GSFC's Space Physics Data Facility's OMNIWeb (or CDAWeb or ftp) service and OMNI data. We thank the institutes who maintain he IMAGE Magnetometer Array. IRM was supported by A Discovery Grant from Canadian NSERC.

The Editor thanks two anonymous reviewers for their assistance in evaluating this paper.

References

Baker, D. N., et al. (2014), An impenetrable barrier to ultrarelativistic electrons in the Van Allen radiation belts, *Nature*, *515*, 531–534, doi:10.1038/nature13956.

Balasis, G., I. A. Daglis, E. Zesta, C. Papadimitriou, M. Georgiou, R. Haagmans, and K. Tsinganos (2012), ULF wave activity during the 2003 Halloween superstorm: Multipoint observations from CHAMP, Cluster and Geotail missions, *Ann. Geophys.*, *30*, 1751–1768, doi:10.5194/angeo-30-1751-2012.

Balasis, G., I. A. Daglis, M. Georgiou, C. Papadimitriou, and R. Haagmans (2013), Magnetospheric ULF wave studies in the frame of Swarm mission: A time-frequency analysis tool for automated detection of pulsations in magnetic and electric field observations, *Earth Planets Space*, *65*, 1385–1398, doi:10.5047/eps.2013.10.003.

Brautigam, D. H., and J. M. Albert (2000), Radial diffusion analysis of outer radiation belt electrons during the October 9, 1990, magnetic storm, *J. Geophys. Res.*, *105*, 291–310, doi:10.1029/1999JA900344.

Brautigam, D. H., G. P. Ginet, J. M. Albert, J. R. Wygant, D. E. Rowland, A. Ling, and J. Bass (2005), CRRES electric field power spectra and radial diffusion coefficients, *J. Geophys. Res.*, *110*, A02214, doi:10.1029/2004JA010612.

Brizard, A. J., and A. A. Chan (2001), Relativistic bounce-averaged quasilinear diffusion equation for low-frequency electromagnetic fluctuations, *Phys. Plasmas*, *8*, 4762–4771, doi:10.1063/1.1408623.

Cahill, L. J. Jr., and J. R. Winckler (1992), Periodic magnetopause oscillations observed with the GOES satellites on March 24, 1991, *J. Geophys. Res.*, *97*, 8239–8243, doi:10.1029/92JA00433.

Fälthammar, C.-G. (1965), Effects of time-dependent electric fields on geomagnetically trapped radiation, *J. Geophys. Res.*, *70*, 2503–2516, doi:10.1029/JZ070i011p02503.

Fei, Y., A. A. Chan, S. R. Elkington, and M. J. Wiltberger (2006), Radial diffusion and MHD particle simulations of relativistic electron transport by ULF waves in the September 1998 storm, *J. Geophys. Res.*, *111*, A12209, doi:10.1029/2005JA011211.

Greenstadt, E. W., J. V. Olson, P. D. Loewen, H. J. Singer, and C. T. Russell (1979), Correlation of PC 3, 4, and 5 activity with solar wind speed, *J. Geophys. Res.*, *84*, 6694–6696, doi:10.1029/JA084iA11p06694.

Hartinger, M., V. Angelopoulos, M. B. Moldwin, K.-H. Glassmeier, and Y. Nishimura (2011), Global energy transfer during a magnetospheric field line resonance, *J. Geophys. Res.*, *38*, L12101, doi:10.1029/2011GL047846.

Huang, C.-L., H. E. Spence, H. J. Singer, and W. J. Hughes (2010), Modeling radiation belt radial diffusion in ULF wave fields: 1. Quantifying ULF wave power at geosynchronous orbit in observations and in global MHD model, *J. Geophys. Res.*, *115*, A06215, doi:10.1029/2009JA014917.

Kepko, L., H. E. Spence, and H. J. Singer (2002), ULF waves in the solar wind as direct drivers of magnetospheric pulsations, *Geophys. Res. Lett.*, *29*(8), 1197, doi:10.1029/2001GL014405.

Kessel, R. L. (2008), Solar wind excitation of Pc5 fluctuations in the magnetosphere and on the ground, *J. Geophys. Res.*, *113*, A04202, doi:10.1029/2007JA012255.

King, J. H., and N. E. Papitashvili (2005), Solar wind spatial scales in and comparisons of hourly Wind and ACE plasma and magnetic field data, *J. Geophys. Res.*, *110*, A02104, doi:10.1029/2004JA010649.

Kivelson, M. G., and D. J. Southwood (1988), Hydromagnetic waves and the ionosphere, *Geophys. Res. Lett.*, *15*, 1271–1274, doi:10.1029/GL015i011p01271.

Li, X., D. N. Baker, T. P. O'Brien, L. Xie, and Q. G. Zong (2006), Correlation between the inner edge of outer radiation belt electrons and the innermost plasmapause location, *Geophys. Res. Lett.*, *33*, L14107, doi:10.1029/2006GL026294.

Loto'Aniu, T. M., I. R. Mann, L. G. Ozeke, A. A. Chan, Z. C. Dent, and D. K. Milling (2006), Radial diffusion of relativistic electrons into the radiation belt slot region during the 2003 Halloween geomagnetic storms, *J. Geophys. Res.*, *111*, A04218, doi:10.1029/2005JA011355.

Lysak, R. L., and D.-H. Lee (1992), Response of the dipole magnetosphere to pressure pulses, *Geophys. Res. Lett.*, *19*, 937–940, doi:10.1029/92GL00625.

Mann, I. R., A. N. Wright, and P. S. Cally (1995), Coupling of magnetospheric cavity modes to field line resonances: A study of resonance widths, *J. Geophys. Res.*, *100*, 19,441–19,456, doi:10.1029/95JA00820.

Mann, I. R., A. N. Wright, K. J. Mills, and V. M. Nakariakov (1999), Excitation of magnetospheric waveguide modes by magnetosheath flows, *J. Geophys. Res.*, *104*, 333–354, doi:10.1029/1998JA900026.

Mann, I. R., et al. (2008), The upgraded CARISMA magnetometer array in the THEMIS Era, *Space Sci. Rev.*, *141*, 413–451, doi:10.1007/s11214-008-9457-6.

Mann, I. R., K. R. Murphy, L. G. Ozeke, I. J. Rae, D. K. Milling, A. Kale, and F. Honary (2012), *The Role of Ultralow Frequency Waves in Radiation Belt Dynamics, Geophys. Monogr. Ser.*, 69–91 pp., vol. 199, AGU, Washington, D. C.

Mathie, R. A., and I. R. Mann (2000), Observations of Pc5 field line resonance azimuthal phase speeds: A diagnostic of their excitation mechanism, *J. Geophys. Res.*, *105*, 10,713–10,728, doi:10.1029/1999JA000174.

O'Brien, T. P., and M. B. Moldwin (2003), Empirical plasmapause models from magnetic indices, *Geophys. Res. Lett.*, *30*(4), 1152, doi:10.1029/2002GL016007.

Ozeke, L. G., I. R. Mann, and I. J. Rae (2009), Mapping guided Alfvén wave magnetic field amplitudes observed on the ground to equatorial electric field amplitudes in space, *J. Geophys. Res.*, *114*, A01214, doi:10.1029/2008JA013041.

Ozeke, L. G., I. R. Mann, K. R. Murphy, I. J. Rae, D. K. Milling, S. R. Elkington, A. A. Chan, and H. J. Singer (2012), ULF wave derived radiation belt radial diffusion coefficients, *J. Geophys. Res.*, *117*, A04222, doi:10.1029/2011JA017463.

Ozeke, L. G., I. R. Mann, K. R. Murphy, I. Jonathan Rae, and D. K. Milling (2014), Analytic expressions for ULF wave radiation belt radial diffusion coefficients, *J. Geophys. Res. Space Physics*, *119*, 1587–1605, doi:10.1002/2013JA019204.

Pahud, D. M., I. J. Rae, I. R. Mann, K. R. Murphy, and V. Amalraj (2009), Ground-based Pc5 ULF wave power: Solar wind speed and MLT dependence, *J. Atmos. Sol. Terr. Phys.*, *71*, 1082–1092, doi:10.1016/j.jastp.2008.12.004.

Rae, I. J., I. R. Mann, K. R. Murphy, L. G. Ozeke, D. K. Milling, A. A. Chan, S. R. Elkington, and F. Honary (2012), Ground-based magnetometer determination of in situ Pc4–5 ULF electric field wave spectra as a function of solar wind speed, *J. Geophys. Res.*, *117*, A04221, doi:10.1029/2011JA017335.

Schulz, M., and L. J. Lanzerotti (1974), *Particle Diffusion in the Radiation Belts*, Physics and Chemistry in Space, vol. 7, Springer-Verlag, Berlin Heidelberg, doi:10.1007/978-3-642-65675-0.

Simms, L. E., V. A. Pilipenko, and M. J. Engebretson (2010), Determining the key drivers of magnetospheric Pc5 wave power, *J. Geophys. Res.*, *115*, A10241, doi:10.1029/2009JA015025.

Takahashi, K., and A. Y. Ukhorskiy (2007), Solar wind control of Pc5 pulsation power at geosynchronous orbit, *J. Geophys. Res.*, *112*, A11205, doi:10.1029/2007JA012483.

Tanskanen, E. I. (2009), A comprehensive high-throughput analysis of substorms observed by IMAGE magnetometer network: Years 1993-2003 examined, *J. Geophys. Res.*, *114*, A05204, doi:10.1029/2008JA013682.

Tu, W., S. R. Elkington, X. Li, W. Liu, and J. Bonnell (2012), Quantifying radial diffusion coefficients of radiation belt electrons based on global MHD simulation and spacecraft measurements, *J. Geophys. Res.*, *117*, A10210, doi:10.1029/2012JA017901.